PCCP

PAPER

View Article Online
View Journal | View Issue

Cite this: *Phys. Chem. Chem. Phys.*, 2023, **25**, 8161

Charge and energy transfer dynamics in single colloidal quantum dots/monolayer MoS_2 heterostructures

Bin Li,[ab] Yuke Gao,[a] Ruixiang Wu,[a] Xiangyang Miao*[a] and Guofeng Zhang*[b]

Received 10th December 2022,
Accepted 22nd February 2023

DOI: 10.1039/d2cp05771a

rsc.li/pccp

The charge and energy transfer dynamics in colloidal CdSeTe/ZnS quantum dots (QDs)/monolayer molybdenum disulfide (MoS_2) heterostructures have been investigated by time-resolved single-dot photoluminescence (PL) spectroscopy. A time-gated method is used to separate the PL photons of single QDs from the PL photons of monolayer MoS_2, which are impossible to be separated by the spectral filter due to their spectral overlap. It is found that the energy transfer from MoS_2 to single QDs increases the exciton generation of the QDs by 37.5% and the energy transfer from single QDs to MoS_2 decreases the PL quantum yield of the QDs by 66.9%. In addition, it is found that MoS_2 increases the discharging rate of single QDs by 59%, while the charging rate remains unchanged. This investigation not only provides valuable insight into the exciton generation and recombination at the single-dot level across such hybrid 0D–2D interfaces but also promotes the application of the hybrid system in various optoelectronic devices.

1. Introduction

Zero-dimensional (0D) colloidal quantum dots (QDs)/two-dimensional (2D) transition metal disulfide (TMD) mixed-dimensional van der Waals heterostructures have attracted a great deal of research interest in both fundamental research and practical applications.[1,2] In the 0D–2D heterostructures, the 0D-QDs have broad tunability of the bandgaps, high absorption cross-sections, and high quantum yields;[3–7] the 2D-TMDs have high transport mobility, direct optical band gap, and reduced dielectric screening.[8–11] Therefore, the 0D–2D van der Waals heterostructures have shown great potential in various optoelectronic applications, such as field-effect transistors, infrared photodetectors, and memory devices.[12–14]

Investigation of charge and energy transfer between 0D-QDs and 2D-TMDs plays an important role in the design and performance improvement of these 0D–2D optoelectronic devices.[15–17] The nonradiative energy transfer from CdSe-based QDs to TMDs has been investigated, revealing how the energy transfer varies with the TMD layer number and temperature.[18–20] The energy transfer from monolayer 2D-TMDs to near-infrared emitting PbS-based 0D-QDs has also been investigated, showing that 58% of the QD photoluminescence (PL) arises due to energy transfer from the monolayer WS_2.[21] The charge transfer from 2D-TMDs to a single layer of CdSe-based QDs has been investigated by femtosecond pump–probe spectroscopy, revealing ultrafast charge transfer from the 2D to the 0D and hybrid exciton formation in the 2D/0D heterostructures.[22] Using single-dot spectroscopy to study the energy transfer and charge transfer dynamics in 2D/0D heterostructures can remove the ensemble averaging effect and obtain the structure and dynamics information of nanomaterials at the level of single particles.[23,24] However, the current problem is that the PL intensity of single QDs is much smaller than that of 2D-TMDs, and the emission spectra of 2D-TMDs overlap with those of most kinds of QDs, especially for CdSe-based QDs.[9,19] Therefore, how to separate the photons emitted by single QDs and 2D-TMDs is still a key problem. This makes it difficult to extract the PL blinking dynamics of single QDs.

The analysis of the PL blinking properties of single QDs can be a good way to obtain the charge transfer dynamics in 2D/0D heterostructures. In the PL trajectory of a single QD, the "bright" states and "dim" states represent the neutral exciton states and charged states, respectively.[25–28] When QDs are charged, the Auger process will consume the formed excitons, resulting in a decrease in PL intensity.[3,29] The charging and discharging process of a single QD leads to the blinking phenomenon. The charge and discharge rates of single QDs can reflect the charge transfer dynamics in 2D/0D heterostructures. As long as the PL photons of single QDs are separated, the study of PL blinking dynamics can be carried out.

In this study, we will investigate energy transfer and charge transfer between CdSeTe/ZnS core/shell QDs and monolayer

[a] *Key Laboratory of Spectral Measurement and Analysis of Shanxi Province, College of Physics and Information Engineering, Shanxi Normal University, Taiyuan, 030031, China. E-mail: xymiao@sxnu.edu.cn*

[b] *State Key Laboratory of Quantum Optics and Quantum Optics Devices, Institute of Laser Spectroscopy, Collaborative Innovation Center of Extreme Optics, Shanxi University, Taiyuan, 030006, China. E-mail: guofeng.zhang@sxu.edu.cn*

molybdenum disulfide (MoS_2) by single-dot PL spectroscopy. Combined with time-tagged, time-resolved, and time-correlated single-photon counting (TTTR-TCSPC) technology, a gating method is used to filter out the MoS_2 emission, thereby extracting the PL photons of a single QD. By comparing the PL blinking trajectories and lifetimes of single QDs on monolayer MoS_2 and silicon, the energy transfer and charge transfer dynamics in the 0D–2D heterostructure were investigated.

2. Materials and methods

The NIR CdSeTe/ZnS core/shell QDs (Qdot® 800ITKTM Organic Quantum Dots) were bought from Thermo Fisher Scientific, the diameter of the core is 6.4 nm and the diameter of the core plus shell is 8.2 nm. The MoS_2 that was prepared by vapor deposition on a silicon wafer was bought from Shenzhen Two-Dimensional New Material Co., Ltd. The average thickness is less than 1 nm. Fig. 1a shows the absorption spectra and PL spectra of the CdSeTe/ZnS core/shell QDs and MoS_2. The spectra of the QD solution in toluene were measured by fluorescence spectrophotometer (F-7000, HITACHI). The spectra of MoS_2 on silicon were measured by a monochromator equipped with a cooled CCD (PIXIS, Princeton Instrument Inc.), and a 532 nm excitation laser. Fig. 1b shows the transmission electron microscope image of the QDs (JEOL-2100F). Fig. 1c shows the optical image of monolayer MoS_2.

To realize the investigation of single QDs, the solution of QDs is appropriately diluted and then spin-coated on the MoS_2 substrate to obtain a 0D–2D hybrid structure. The areal density of the QDs was kept below 0.1 μm^{-2} to allow us to observe isolated QDs with a confocal microscope. We have also prepared the contrast sample with only single QDs on a silicon wafer as a control experiment. A home built confocal scanning microscope was used to measure the PL properties of single QDs on monolayer MoS_2 at room temperature. The single QDs were excited by a 532 nm pulsed laser (WL-SC-400-15-PP, NKT Photonics) with a pulse width of about 90 ps and a repetition rate of 5 MHz and the PL was collected by an objective (Nikon, 100×, 0.9 NA). After passing through a dichroic mirror (Semrock) and a long-pass filter (Semrock), the PL photons were focused into a pinhole of 0.1 mm for spatial filtering, and then split by a 50/50 beamsplitter cube into two beams and finally detected by a pair of single-photon avalanche diode detectors (SPCM-AQR-15, PerkinElmer). The arrival time of each PL photon and the synchronization of the pulse laser were recorded by a TTTR-TCSPC data acquisition card (HydraHarp 400). Based on the absorption and PL spectra in Fig. 1a, we added a long-pass filter of 736 nm to remove the PL of monolayer MoS_2. Nevertheless, the remaining PL of monolayer MoS_2 is still very significant and is more than the PL of a single QD due to their partial spectral overlap. According to the arrival time of each PL photon and the synchronization information of the laser pulse, we use a time-gated method[30,31] to separate the PL photons of the QDs and monolayer MoS_2, as schematically shown in Fig. 2a. The time-gated method allows for selective analysis of only photons that arrive after a certain time delay following the sync pulse, which enables the construction of a time-gated $g^{(2)}$ function and PL intensity.[30]

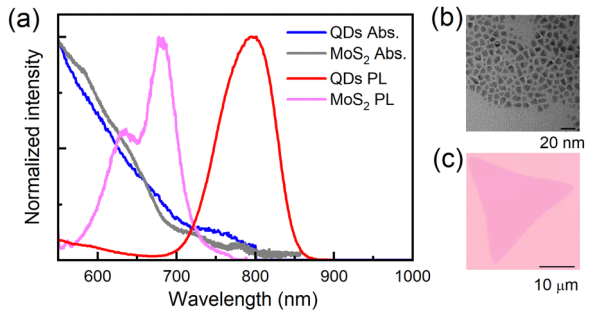

Fig. 1 (a) Absorption and PL spectra of CdSeTe/ZnS QDs and monolayer MoS_2. (b) Transmission electron microscope images of the QDs. (c) The optical image of monolayer MoS_2.

3. Results and discussion

According to the spectral overlap between the absorption spectra and the PL spectra shown in Fig. 1a, the energy transfer from monolayer MoS_2 to QDs and the energy transfer from QDs to monolayer MoS_2 simultaneously take place in the 0D–2D heterostructure. The energy transfer from monolayer MoS_2 to QDs can enhance the exciton generation of the QDs,[21,32,33] but does not affect the exciton recombination dynamics of the QDs. While the energy transfer from QDs to MoS_2 can decrease the exciton lifetime of the QDs.[20] Therefore, single-QD spectroscopy is helpful to separately investigate the two energy transfer dynamics in a 0D–2D mixed structure. In addition, the CdSeTe/ZnS core/shell QDs have strong electron–hole pair confinement and a thick shell, so the charge transfer effect between the QD core and MoS_2 is inefficient.[20] However, the charge transfer in the 0D–2D heterostructure still exists according to the study on the dynamics of PL blinking of single QDs.

The work began by finding single QDs. The confocal scanning PL intensity image of single QDs on monolayer MoS_2 is shown in Fig. 2b. The PL intensity of MoS_2 is much higher than that of single QDs, so the PL signals of single QDs are submerged. Fig. 2c is obtained by rescanning the red square area in Fig. 2b by adding a 736 nm long-pass filter to remove most of the PL of MoS_2, but the outline of single QDs still can't be seen. The corresponding PL lifetime image (Fig. 2d) shows that the lifetime of QDs on monolayer MoS_2 (orange) is shorter than that on silicon (red). In addition, the PL lifetime of MoS_2 is about 0.1 ns (corresponding to previous work[34]) which is much shorter than that of the QDs. Based on the above results, we set a time-gate of 5 ns to filter out PL photons of monolayer MoS_2 and the corresponding time-gated PL intensity image was obtained, as shown in Fig. 2e. The outline of QDs is clearly presented, and the single QDs are easily found. The single QDs marked with yellow circles in Fig. 2d confirm that the distance between single QDs is sufficiently far apart to allow us to obtain pure single QD emission. For confirming that the QDs on monolayer MoS_2 are individual, we use the photon correlation function ($g^{(2)}$)

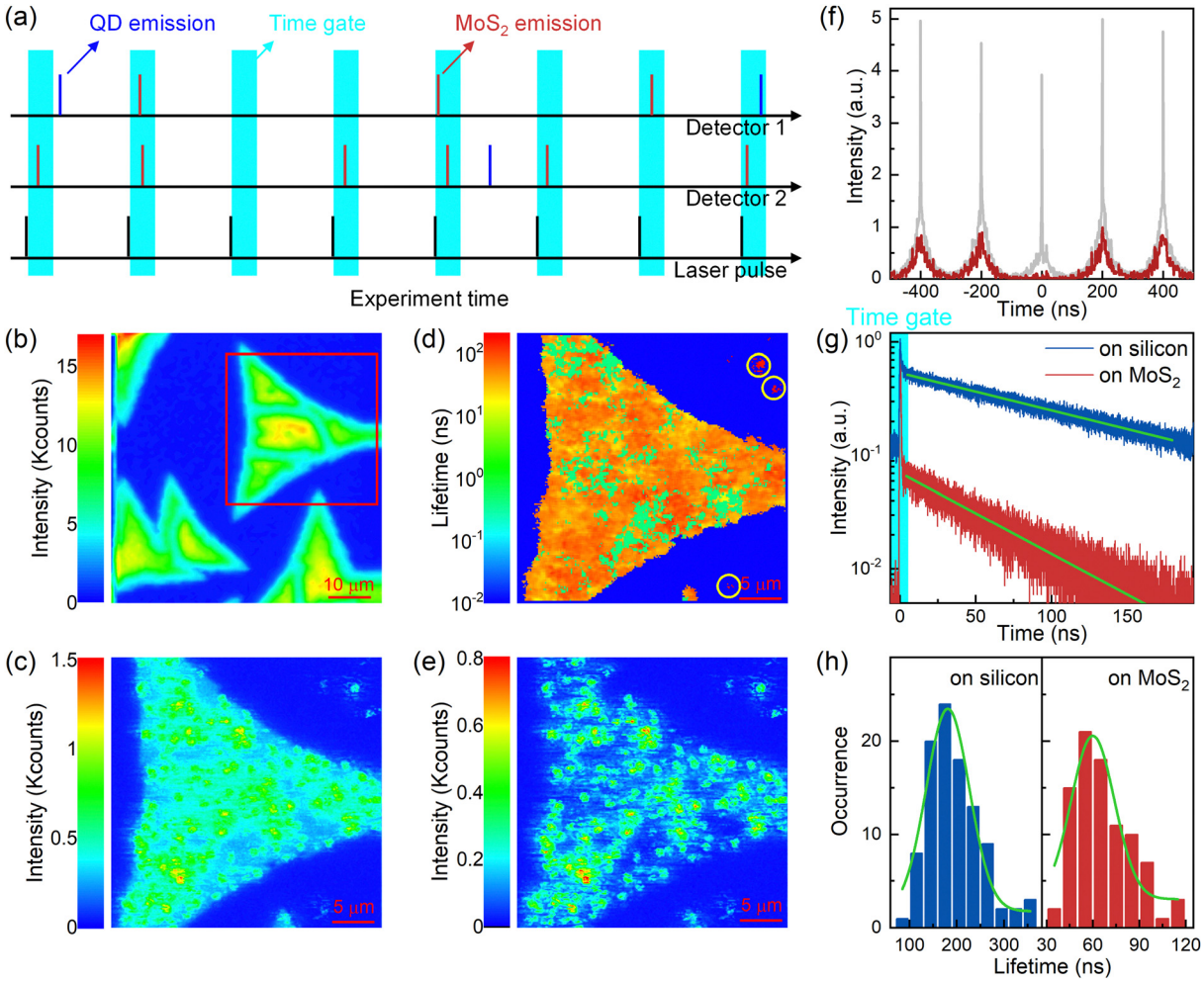

Fig. 2 (a) Schematic of the PL signals recorded by TTTR-TCSPC technology. Laser pulses come at regular intervals. The red bars and blue bars correspond to photons emitted from MoS_2 and single QDs, respectively. For our analysis we set a time gate (cyan shaded area) after the laser pulse to remove the MoS_2 emission. (b and c) PL intensity images of single QDs on monolayer MoS_2 with long-pass filters of 655 nm (b) and 736 nm (c). (d) Corresponding PL lifetime images with the long-pass filter of 736 nm. The areas marked by yellow circles are single QDs on silicon. (e) Corresponding time-gated PL intensity image with delay time of 5 ns and the emission filter of 736 nm. (f) The grey line is a typical $g^{(2)}$ curve of a single QD on monolayer MoS_2, and the red line is the corresponding time-gated $g^{(2)}$ curve with a threshold of 5 ns. (g) PL decays and exponential fits for single QDs on silicon and MoS_2, respectively. Setting the time-gate at 5 ns can remove the effect of MoS_2 emission. (h) Histograms of lifetimes of single-exciton states for single QDs on silicon and MoS_2 with Gaussian fitting (green curves), respectively.

method to recognize a single QD.[35] However, the $g^{(2)}(0)$ value is very large for the QDs on monolayer MoS_2 (grey line in Fig. 2f), and it is impossible to recognize single QDs by the $g^{(2)}$ method due to the influence of the PL of MoS_2. Here, we use the time-gated $g^{(2)}$ method to recognize single QDs.[35] A typical time-gated $g^{(2)}$ curve (red line) is shown in Fig. 2f, and the areal ratio of the central peak to the side peaks is well below 0.5, implying that our measurements are from isolated single QDs.

After recognizing the single QDs, we recorded the arrival time of each PL photon from a single QD with TTTR-TCSPC technology to investigate the charge and energy transfer dynamics in the 0D–2D heterostructure. The typical PL decay curves of single QDs on silicon (blue) and monolayer MoS_2 (red) are shown in Fig. 2g. The PL decays can be fitted well by using single exponential functions (green curves), which can be attributed to the relaxation of single exciton states.[36] The histograms of the single exciton lifetime values for ~100 single QDs on silicon and MoS_2 are shown in Fig. 2h. The Gaussian fitting yields the mean values of 181.1 and 59.9 ns for single QDs on silicon and on monolayer MoS_2, respectively. Therefore, the exciton lifetimes of QDs on MoS_2 are reduced to 33.1% that of QDs on silicon. The value of 181.1 ns corresponds to the radiative lifetime of single excitons in single QDs, which is close to the reported silicon,[37] and thus the radiative rate (k_r) of a single exciton of QDs is

$$k_r = \frac{1}{181.1\ \text{ns}} = 5.5 \times 10^6\ \text{s}^{-1} \quad (1)$$

The reduced lifetime of QDs on MoS_2 indicates the existence of Förster resonance energy transfer from the QDs to MoS_2 and the energy transfer rate (k_{ET}) can be calculated by[38]

$$k_{ET} = k - k_r = \frac{1}{59.9\ \text{ns}} - \frac{1}{181.1\ \text{ns}} = 1.1 \times 10^7\ \text{s}^{-1}, \quad (2)$$

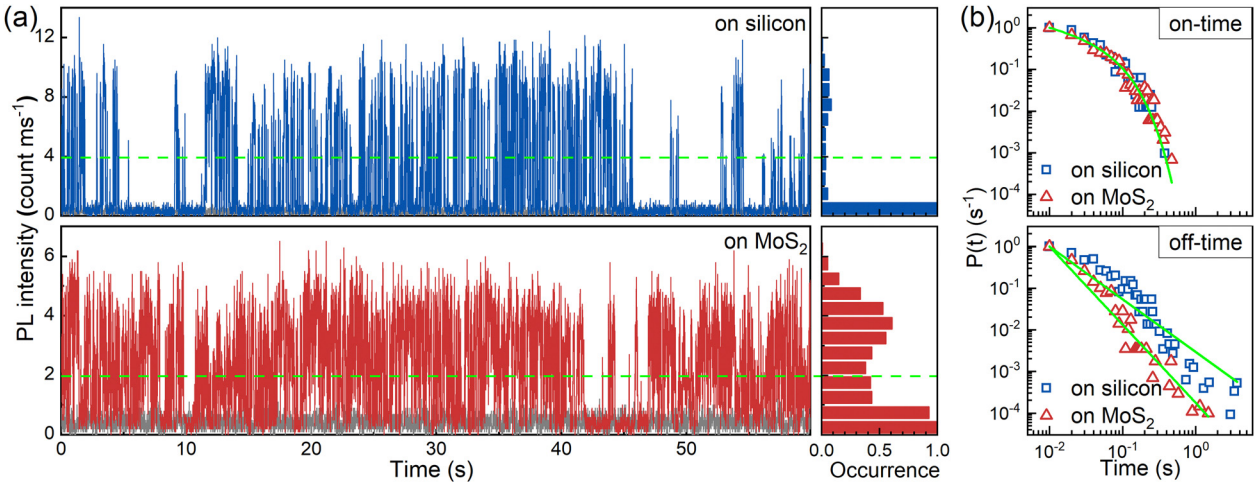

Fig. 3 (a) Typical PL intensity trajectories for the single QDs on silicon (blue line) and monolayer MoS_2 (red line) with binning time of 10 ms, respectively. The PL photons of MoS_2 have been removed by the time-gated method. The silver-gray lines represent background. Corresponding PL intensity histograms are shown in the right panels. (b) Normalized probability densities of on- and off-time for single QDs on silicon and monolayer MoS_2, respectively. The solid lines are best fits by (truncated) power law functions.

where k is the exciton recombination rate of the QDs on MoS_2. Because of the energy transfer from the QDs to MoS_2, the PL intensity of the QDs on MoS_2 should decrease to k_r/k = 33.1% of that on silicon. However, measurements of the PL intensity of single QDs did not agree with this value, which mean that the energy transfer from MoS_2 to QDs also exists, see next paragraph.

Fig. 3a shows two typical PL intensity trajectories and the corresponding PL intensity histograms for single QDs on silicon and monolayer MoS_2 (the PL photons of MoS_2 have been removed by the time-gated method), respectively. The PL intensities of ~100 single QDs on silicon and on MoS_2 are ~11 K and ~5 K, respectively. The experimental results show that the PL intensity of single QDs on monolayer MoS_2 is 45.5% (>33.1%) of that on silicon, which is proof of the existence of energy transfer from monolayer MoS_2 to single QDs. In addition, the energy transfer increases the exciton generation of single QDs by 45.5%/33.1%–100% = 37.5%. Finally, the decrease of PL intensity of single QDs on monolayer MoS_2 reveals that the 0D to 2D energy transfer is more prominent in the CdSeTe/ZnS QDs/monolayer MoS_2 hybrid system.

Fig. 3a also shows that the PL intensity of the single QDs fluctuates between bright (on) and dark (off) states, which is called PL blinking.[39–42] The PL blinking can be explained by the charging model, which originates from photoionization (charging) and neutralization (discharging).[39,43] In a neutral QD, on-state emission originates from the radiative recombination of the exciton. When the electron of the exciton is captured by the surface traps, the QD will be positively charged. The extra hole can initiate nonradiative Auger recombination, which leads to a decrease in PL intensity (called the off-state). When the electron is released from the surface traps, the QD will be discharged and the PL intensity will return to the on-state. When the electron in the core is captured by the surface traps, it is closer to MoS_2, so the charge transfer occurs more easily and affects the blinking properties of the single QD. The PL intensity histograms in the right panels of Fig. 3a reveal that the PL of a single QD on MoS_2 has more on-state compared with that on silicon. The increase in the on-state may originate from the decrease of the charging rate or the increase of the discharging rate. In order to quantitatively investigate the effect of MoS_2 on the charging and discharging process of single QDs, we calculate the statistical distribution[44] of on- and off-time of PL intensity traces.

The normalized on- and off-time probability densities[45–47] are the fingerprint of QD blinking studies to investigate and compare the blinking activities of single QDs on silicon and monolayer MoS_2. According to the two peaks of PL intensity histograms in Fig. 3a, a threshold intensity (green dotted lines) was set to separate the on- and off-state of the PL trajectories. Then, the on- and off-time probability densities $P_{on}(t)$ and $P_{off}(t)$ can be derived from the PL intensity trajectories, as shown in Fig. 3b. The on- and off-time probability density distributions can be fitted by an exponentially truncated power law:

$$P_{on}(t) = A_{on}t^{-\alpha}\exp(-\mu t) \quad (3)$$

and power law

$$P_{off}(t) = A_{off}t^{-\beta}, \quad (4)$$

respectively, where A_{on} and A_{off} are amplitudes, α and β are the power law exponents, and μ is the saturation rate.[48] The corresponding fitting parameters have been obtained by fitting of ~60 single QDs on silicon and monolayer MoS_2, respectively, as shown in Table 1. Single QDs on monolayer MoS_2 have a larger β value than that of single QDs on silicon, while α and μ have similar values. According to the fitting parameters, the charging rate ($k_{on\to off}$) and discharging rate ($k_{off\to on}$)[49] for ~60 single QDs on silicon and MoS_2 can also be obtained by

$$\frac{1}{k_{on\to off}} = \int_{0.01}^{\infty} P_{on}(t)\mathrm{d}t, \quad (5)$$

Table 1 Normalized on- and off-time probability densities for ~60 single QDs on silicon and monolayer MoS_2, respectively

	α	$1/\mu$ (ms)	β	$k_{on\to off}$ (s^{-1})	$k_{off\to on}$ (s^{-1})
QDs (on silicon)	0.55 ± 0.35	53.63 ± 42.33	1.16 ± 0.27	21.8	5.8
QDs (on MoS_2)	0.62 ± 0.25	65.86 ± 6.11	1.72 ± 0.17	20.0	14.2

and

$$\frac{1}{k_{off\to on}} = \int_{0.01}^{\infty} P_{off}(t)\mathrm{d}t, \quad (6)$$

respectively, as shown in Table 1. The results show that the discharging rate of a single QD on monolayer MoS_2 is decreased by 59% compared to that on silicon, while the charging rate remains unchanged. This is because the electron in the surface traps can be transferred to MoS_2 and then recombine with the hole in the valence band of QD. Therefore, the charge transfer in 0D–2D heterostructures increases the bright state ratio of single QDs to a certain extent, but the blinking rate does not decrease significantly.

Based on the above experimental results, we use an external electron transfer model to describe the energy and charge transfer processes as well as the suppression of the off-state of CdSeTe/ZnS QDs by monolayer MoS_2, as shown in Fig. 4. The conduction and valence band positions for CdSeTe/ZnS QD and monolayer MoS_2 are obtained from previous reports.[49,50] The energy transfer from monolayer MoS_2 to single QDs increases the probability of exciton generation of the QDs and thus increases the PL intensity of a single QD. Moreover, the energy transfer from single QDs to monolayer MoS_2 can cause non-radiative relaxation and decrease the PL intensity of the single QD. The results show that the 0D to 2D energy transfer process is more prominent than the 2D to 0D energy transfer process in the hybrid system. In addition, the monolayer MoS_2 can provide an electron transfer pathway from the trap state of the single QD. Thus, the PL blinking of single QDs is influenced when contacted with monolayer MoS_2. According to the experimental results, we can calculate the charge transfer rate (k_{CT}) from monolayer MoS_2 to single QDs. For an isolated single QD,

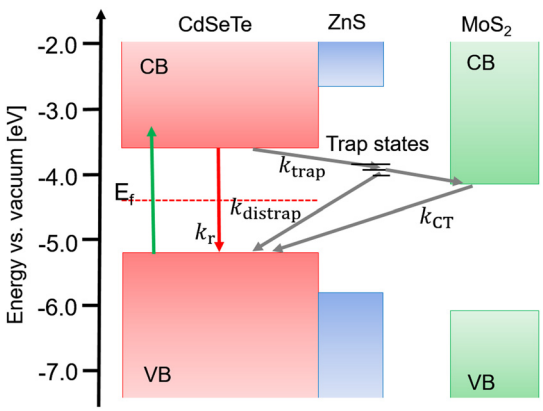

Fig. 4 Schematic of the external electron transfer model. CB and VB are the conduction band and valence band, respectively. E_f is the Fermi level. k_r, k_{trap}, $k_{distrap}$, and k_{CT} are radiative rate, trapping rate, distrapping rate and charge transfer rate, respectively.

Table 2 Calculated parameters involved in the heterostructure

k_r (s^{-1})	k_{trap} (s^{-1})	$k_{distrap}$ (s^{-1})	k_{ET} (s^{-1})	k_{CT} (s^{-1})
5.5×10^6	21.8	5.8	1.1×10^7	8.4

the charging ($k_{on\to off}$) and discharging rates ($k_{off\to on}$) are equal to the trapping (k_{trap}) and distrapping rates ($k_{distrap}$), respectively.[39] Therefore, the values of k_{trap} and $k_{distrap}$ are obtained as 21.8 s^{-1} and 5.8 s^{-1}, respectively. Then, the value of k_{CT} is $k_{off\to on}^{on\ MoS_2} - k_{distrap} = 14.2\ s^{-1} - 5.8\ s^{-1} = 8.4\ s^{-1}$. A summary table of calculated parameters for single QDs on monolayer MoS_2 obtained in this work is presented in Table 2.

4. Conclusions

We have studied the charge and energy transfer dynamics between CdSeTe/ZnS QDs and monolayer MoS_2. By removing the PL photons of MoS_2 by a suitable time-gate, the PL of single QDs can be obtained. By comparing the PL lifetime and PL intensity trajectories of single QDs on silicon and monolayer MoS_2, it was found that the energy transfer from MoS_2 to single QDs increases the exciton generation of single QDs by 37.5% and the energy transfer from single QDs to MoS_2 decreases the PL intensity of single QDs by 66.9%. Therefore, the 0D to 2D energy transfer process is more prominent than the 2D to 0D energy transfer process in the hybrid system. Moreover, the discharging rate of single QDs on monolayer MoS_2 is increased by 59% compared to that on silicon, while the charging rate remains unchanged. By combining the external electron transfer mode, the various parameters involved have been obtained to reveal the energy and electron transfer processes in the 0D–2D heterostructure. This investigation not only provides valuable insight into the exciton generation and recombination at the single-dot level across such hybrid 0D–2D interfaces, but also promotes the application of the hybrid system in various optoelectronic devices.

Author contributions

G.Z. conceived and designed the experiments. B.L. performed the experiments and analyzed the data. B.L. and G.Z. co-wrote the manuscript. All authors discussed the results and commented on the manuscript at all stages.

Conflicts of interest

There are no conflicts to declare.

Acknowledgements

This work was supported by the Natural Science Foundation of China (No. 62075120, 61805134, 11974229, 62127817), Fundamental Research Program of Shanxi Province (No. 202103021223254, 201801D221016), and PTIT, Scientific and Technological Innovation Programs of Higher Education Institutions in Shanxi (Grant No. 2021L257, 2020L0235, 2022L267).

Notes and references

1 D. Jariwala, T. J. Marks and M. C. Hersam, *Nat. Mater.*, 2017, **16**, 170–181.
2 L. L. Luo, P. X. Wang, X. Y. Geng, Y. T. Liu, R. I. Eglitis, H. Q. Xia, X. Y. Lai and X. Wang, *Phys. Chem. Chem. Phys.*, 2022, **24**, 8529–8536.
3 F. P. García de Arquer, D. V. Talapin, V. I. Klimov, Y. Arakawa, M. Bayer and E. H. Sargent, *Science*, 2021, **373**, 640.
4 J. M. Pietryga, Y. S. Park, J. H. Lim, A. F. Fidler, W. K. Bae, S. Brovelli and V. I. Klimov, *Chem. Rev.*, 2016, **116**, 10513–10622.
5 G. H. Carey, A. L. Abdelhady, Z. Ning, S. M. Thon, O. M. Bakr and E. H. Sargent, *Chem. Rev.*, 2015, **115**, 12732–12763.
6 F. Zhang, H. Zhong, C. Chen, X.-g Wu, X. Hu, H. Huang, J. Han, B. Zou and Y. Dong, *ACS Nano*, 2015, **9**, 4533–4542.
7 J. Baronnier, B. Mahler, O. Boisron, C. Dujardin, F. Kulzer and J. Houel, *Phys. Chem. Chem. Phys.*, 2021, **23**, 22750–22759.
8 K. F. Mak, C. Lee, J. Hone, J. Shan and T. F. Heinz, *Phys. Rev. Lett.*, 2010, **105**, 136805.
9 Q. H. Wang, K. Kalantar-Zadeh, A. Kis, J. N. Coleman and M. S. Strano, *Nat. Nanotechnol.*, 2012, **7**, 699–712.
10 U. Yorulmaz, D. Šabani, M. Yagmurcukardes, C. Sevik and M. V. Milošević, *Phys. Chem. Chem. Phys.*, 2022, **24**, 29406–29412.
11 X. Liang, C. Qin, Y. Gao, S. Han, G. Zhang, R. Chen, J. Hu, L. Xiao and S. Jia, *Nanoscale*, 2021, **13**, 8966–8975.
12 C. Hu, D. Dong, X. Yang, K. Qiao, D. Yang, H. Deng, S. Yuan, J. Khan, Y. Lan, H. Song and J. Tang, *Adv. Funct. Mater.*, 2017, **27**, 1603605.
13 S. Goossens, G. Navickaite, C. Monasterio, S. Gupta, J. J. Piqueras, R. Pérez, G. Burwell, I. Nikitskiy, T. Lasanta, T. Galán, E. Puma, A. Centeno, A. Pesquera, A. Zurutuza, G. Konstantatos and F. Koppens, *Nat. Photonics*, 2017, **11**, 366–371.
14 Q. Wang, Y. Wen, K. Cai, R. Cheng, L. Yin, Y. Zhang, J. Li, Z. Wang, F. Wang, F. Wang, T. A. Shifa, C. Jiang, H. Yang and J. He, *Sci. Adv.*, 2018, **4**, 7916.
15 M. Li, J. Chen, P. K. Routh, P. Zahl, C. Nam and M. Cotlet, *Adv. Funct. Mater.*, 2018, **28**, 1707558.
16 H. Li, X. Zheng, Y. Liu, Z. Zhang and T. Jiang, *Nanoscale*, 2018, **10**, 1650–1659.
17 Y. Zhang, W. Xiu, Y. Sun, D. Zhu, Q. Zhang, L. Yuwen, L. Weng, Z. Teng and L. Wang, *Nanoscale*, 2017, **9**, 15835–15845.
18 H. D. Zang, P. K. Routh, Y. Huang, J. S. Chen, E. Sutter, P. Sutter and M. Cotlet, *ACS Nano*, 2016, **10**, 4790–4796.
19 S. Sampat, T. L. Guo, K. H. Zhang, J. A. Robinson, Y. Ghosh, K. P. Acharya, H. Htoon, J. A. Hollingsworth, Y. N. Gartstein and A. V. Malko, *ACS Photonics*, 2016, **3**, 708–715.
20 J. Li, W. Zhang, Y. Zhang, H. Lei and B. Li, *Nano Res.*, 2016, **9**, 2623–2631.
21 A. O. A. Tanoh, N. Gauriot, G. Delport, J. Xiao, R. Pandya, J. Sung, J. Allardice, Z. Li, C. A. Williams, A. Baldwin, S. D. Stranks and A. Rao, *ACS Nano*, 2020, **14**, 15374–15384.
22 A. Boulesbaa, K. Wang, M. Mahjouri-Samani, M. Tian, A. A. Puretzky, I. Ivanov, C. M. Rouleau, K. Xiao, B. G. Sumpter and D. B. Geohegan, *J. Am. Chem. Soc.*, 2016, **138**, 14713–14719.
23 J. Zhou, A. I. Chizhik, S. Chu and D. Jin, *Nature*, 2020, **579**, 41–50.
24 B. Li, G. Zhang, R. Chen, C. Qin, J. Hu, L. Xiao and S. Jia, *Acta Phys. Sin.*, 2022, **71**, 067802.
25 X. Han, G. Zhang, B. Li, C. Yang, W. Guo, X. Bai, P. Huang, R. Chen, C. Qin, J. Hu, Y. Ma, H. Zhong, L. Xiao and S. Jia, *Small*, 2020, **16**, 2005435.
26 G. Zhang, Y. Peng, H. Xie, B. Li, Z. Li, C. Yang, W. Guo, C. Qin, R. Chen, Y. Gao, Y. Zheng, L. Xiao and S. Jia, *Front. Phys.*, 2019, **14**, 23605.
27 B. Li, H. Huang, G. Zhang, C. Yang, W. Guo, R. Chen, C. Qin, Y. Gao, V. P. Biju, A. L. Rogach, L. Xiao and S. Jia, *J. Phys. Chem. Lett.*, 2018, **9**, 6934–6940.
28 Z. Li, G. Zhang, B. Li, R. Chen, C. Qin, Y. Gao, L. Xiao and S. Jia, *Appl. Phys. Lett.*, 2017, **111**, 153106.
29 E. M. Thomas, S. Ghimire, R. Kohara, A. N. Anil, K.-I. Yuyama, Y. Takano, K. G. Thomas and V. Biju, *ACS Nano*, 2018, **12**, 9060–9069.
30 B. D. Mangum, Y. Ghosh, J. A. Hollingsworth and H. Htoon, *Opt. Express*, 2013, **21**, 7419–7426.
31 T. Hartsfield, M. Gegg, P. H. Su, M. R. Buck, J. A. Hollingsworth, C. K. Shih, M. Richter, H. Htoon and X. Q. Li, *ACS Photonics*, 2016, **3**, 1085–1089.
32 B. Li, G. Zhang, Y. Zhang, C. Yang, W. Guo, Y. Peng, R. Chen, C. Qin, Y. Gao, J. Hu, R. Wu, J. Ma, H. Zhong, Y. Zheng, L. Xiao and S. Jia, *J. Phys. Chem. Lett.*, 2020, **11**, 10425–10432.
33 X. Liang, C. Qin, Z. Qiao, W. Kang, H. Yin, S. Dong, X. Li, S. Wang, X. Su, G. Zhang, R. Chen, J. Hu, L. Xiao and S. Jia, *Opt. Express*, 2022, **30**, 26557–26569.
34 T. Wang, Y. Zhang, Y. Liu, J. Li, D. Liu, J. Luo and K. Ge, *J. Phys. Chem. C*, 2018, **122**, 18651–18658.
35 B. Li, G. Zhang, C. Yang, Z. Li, R. Chen, C. Qin, Y. Gao, H. Huang, L. Xiao and S. Jia, *Opt. Express*, 2018, **26**, 4674–4685.
36 C. Yang, G. Zhang, L. Feng, B. Li, Z. Li, R. Chen, C. Qin, Y. Gao, L. Xiao and S. Jia, *Opt. Express*, 2018, **26**, 11889–11902.
37 S. W. Feng, C. Y. Cheng, C. Y. Wei, J. H. Yang, Y. R. Chen, Y. W. Chuang, Y. H. Fan and C. S. Chuu, *Phys. Rev. Lett.*, 2017, **119**, 143601.
38 B. Li, R. Chen, C. Qin, C. Yang, W. Guo, X. Han, Y. Gao, G. Zhang, L. Xiao and S. Jia, *Appl. Phys. Express*, 2019, **12**, 112003.
39 R. Y. Meng, H. Y. Qin, Y. Niu, W. Fang, S. Yang, X. Lin, H. J. Cao, J. L. Ma, W. Z. Ling, L. M. Tong and X. G. Peng, *J. Phys. Chem. Lett.*, 2016, **7**, 5176–5182.
40 Z. Hu, S. Liu, H. Qin, J. Zhou and X. Peng, *J. Am. Chem. Soc.*, 2020, **142**, 4254–4264.
41 J.-S. Chen, H. Zang, M. Li and M. Cotlet, *Chem. Commun.*, 2018, **54**, 495–498.

42 L. Hou, C. Zhao, X. Yuan, J. Zhao, F. Krieg, P. Tamarat, M. V. Kovalenko, C. Guo and B. Lounis, *Nanoscale*, 2020, **12**, 6795–6802.
43 J. Li, D. Wang, G. Zhang, C. Yang, W. Guo, X. Han, X. Bai, R. Chen, C. Qin, J. Hu, L. Xiao and S. Jia, *Nano Res.*, 2022, **15**, 7655–7661.
44 C. Yang, R. Xiao, S. Zhou, Y. Yang, G. Zhang, B. Li, W. Guo, X. Han, D. Wang, X. Bai, J. Li, R. Chen, C. Qin, J. Hu, L. Feng, L. Xiao and S. Jia, *ACS Photonics*, 2021, **8**, 2538–2547.
45 D. Roy, S. Mandal, C. K. De, K. Kumar and P. K. Mandal, *Phys. Chem. Chem. Phys.*, 2018, **20**, 10332–10344.
46 L. Chouhan, S. Ito, E. M. Thomas, Y. Takano, S. Ghimire, H. Miyasaka and V. Biju, *ACS Nano*, 2021, **15**, 2831–2838.
47 X. Bai, H. Li, Y. Peng, G. Zhang, C. Yang, W. Guo, X. Han, J. Li, R. Chen, C. Qin, J. Hu, G. Yang, H. Zhong, L. Xiao and S. Jia, *J. Phys. Chem. C*, 2022, **126**, 2699–2707.
48 W. Guo, J. Tang, G. Zhang, B. Li, C. Yang, R. Chen, C. Qin, J. Hu, H. Zhong, L. Xiao and S. Jia, *J. Phys. Chem. Lett.*, 2021, **12**, 405–412.
49 B. Li, G. Zhang, Z. Wang, Z. Li, R. Chen, C. Qin, Y. Gao, L. Xiao and S. Jia, *Sci. Rep.*, 2016, **6**, 32662.
50 S. Roy, G. P. Neupane, K. P. Dhakal, J. Lee, S. J. Yun, G. H. Han and J. Kim, *J. Phys. Chem. C*, 2017, **121**, 1997–2004.